The Role of the Gas Phase in Graphene Formation by CVD on Copper

Pierre Trinsoutrot, Caroline Rabot, Hugues Vergnes, Alexandru Delamoreanu, Aziz Zenasni, Brigitte Caussat

▶ **To cite this version:**

Pierre Trinsoutrot, Caroline Rabot, Hugues Vergnes, Alexandru Delamoreanu, Aziz Zenasni, et al.. The Role of the Gas Phase in Graphene Formation by CVD on Copper. Chemical Vapor Deposition, 2014, 20 (1-2-3), pp.51-58. 10.1002/cvde.201307075 . hal-01889823

HAL Id: hal-01889823
https://hal.science/hal-01889823

Submitted on 8 Oct 2018

HAL is a multi-disciplinary open access archive for the deposit and dissemination of scientific research documents, whether they are published or not. The documents may come from teaching and research institutions in France or abroad, or from public or private research centers.

L'archive ouverte pluridisciplinaire **HAL**, est destinée au dépôt et à la diffusion de documents scientifiques de niveau recherche, publiés ou non, émanant des établissements d'enseignement et de recherche français ou étrangers, des laboratoires publics ou privés.

Open Archive Toulouse Archive Ouverte (OATAO)

OATAO is an open access repository that collects the work of Toulouse researchers and makes it freely available over the web where possible

This is an author's version published in: **http://oatao.univ-toulouse.fr/20303**

Official URL: https://doi.org/10.1002/cvde.201307075

To cite this version:

Trinsoutrot, Pierre and Rabot, Caroline and Vergnes, Hugues and Delamoreanu, Alexandru and Zenasni, Aziz and Caussat, Brigitte *The Role of the Gas Phase in Graphene Formation by CVD on Copper*. (2014) Chemical Vapor Deposition, 20 (1-2-3). 51-58. ISSN 0948-1907

Any correspondence concerning this service should be sent to the repository administrator: tech-oatao@listes-diff.inp-toulouse.fr

DOI: 10.1002/cvde.201307075

Full Paper

The Role of the Gas Phase in Graphene Formation by CVD on Copper**

By *Pierre Trinsoutrot, Caroline Rabot, Hugues Vergnes, Alexandru Delamoreanu, Aziz Zenasni,* and *Brigitte Caussat**

Graphene synthesis on copper foils is experimentally studied at 1000°C under various methane partial pressures. A decrease in the carbon supply permits the formation of larger graphene flakes with fewer layers and crystalline defects. An influence of the copper foil confinement on graphene nucleation and growth is shown. Then, methane pyrolysis is simulated using the Fluent Ansys® code. The model shows that, at 1000°C, CH_4 is decomposed to form gaseous saturated and unsaturated species. This means that two types of unsaturated species can co-exist during graphene synthesis, the first one arising in the reactor volume from methane pyrolysis, and the second one only forming in the vicinity of copper, thanks to its catalytic activity.

Keywords: Catalytic CVD, CFD, Copper, Graphene, Methane

1. Introduction

During the past 40 years, the fields of electronics, energy, and communication devices have experienced an unbelievable evolution. To continue this progress, the development of multifunctional materials presenting a broad range of properties, such as high electric and thermal conductivities, high transparency, and good mechanical properties, is needed. Graphene, a hexagonal arrangement of carbon atoms forming a one-atom thick planar sheet could match these demands. Several methods can be used for graphene synthesis. Historically graphene was produced by micromechanical cleavage.[1] Graphene obtained in this case presents exceptional properties, in particular an electron mobility of 120 000 $cm^2\ V^{-1}\ s^{-1}$.[2] This method is, however, incompatible with industrial applications as it is not scalable. Alternative synthesis methods were then developed to meet industrial requirements, in particular thermal decomposition of SiC,[3,4] reduction of graphene oxide,[5] and transition metal-catalyzed CVD.[6–10] CVD, because of the high quality and the large surfaces of graphene it produces and its low processing costs, seems to be the process most compatible with industrial requirements. Indeed, 30 inch graphene films with an electronic conductivity of 7350 $cm^2\ V^{-1}\ s^{-1}$, an electrical resistance of 30 Ω per sq, and a transparency of 90% have already been obtained by CVD.[11] These values are, however, still far from the theoretical ones announced by physicists, because graphene grows as randomly oriented domains in which scattering at the boundaries leads to less interesting physical properties. The CVD formation of graphene on Cu substrates has long been considered to be surface-mediated and self-limiting due to the very low carbon solubility in Cu, thus leading to single layer formation,[12,13] although numerous studies have shown that this is true in only a small window of deposition conditions, especially regarding methane partial pressure.[14,15] As a consequence, the control of graphene thickness and crystalline quality on large surface areas still remains elusive and needs a better understanding of the mechanisms of graphene nucleation and growth.

In this framework, the present study, by combining experimental and modeling analyses, provides new insights into the role of the gas phase in graphene formation. First, we investigated experimentally graphene synthesis at 1000°C on copper foils under various methane partial pressures. Second, with the knowledge gained from the experimental study, we looked for a deeper understanding by modeling methane pyrolysis into the CVD reactor using the computational fluid dynamics (CFD) Fluent Ansys code.

2. Results and Discussion

First, two total pressures, 0.5 and 700 Torr, were studied under identical operating conditions. The methane flow rate was fixed at 4 sccm, corresponding to methane partial pressures equal to 4.7 mTorr and 6.6 Torr, respectively. As shown in Figures 1a and 1b, graphene nuclei of spheroid

[*] P. Trinsoutrot, Dr. H. Vergnes, Prof. B. Caussat
Université de Toulouse, Laboratoire de Génie Chimique, ENSIACET/INP Toulouse UMR CNRS 5503 4 allée Émile Monso BP 44362, 31432 Toulouse Cedex 4 (France)
E-mail: Brigitte.Caussat@ensiacet.fr
Dr. C. Rabot, Dr. A. Delamoreanu[+], Dr. A. Zenasni
CEA, LETI, MINATEC Campus 17 rue des Martyrs, 38054 GRENOBLE Cedex 9 (France)
[+] Present address: UJF-Grenoble 1/CNRS/CEA LTM 17 rue des Martyrs, 38054 GRENOBLE Cedex 9 (France)

[**] The work was supported by the FP7-NMP GRENADA European project. The authors acknowledge M. Molinier and E. Prevot from LGC/INP de Toulouse, for technical support.

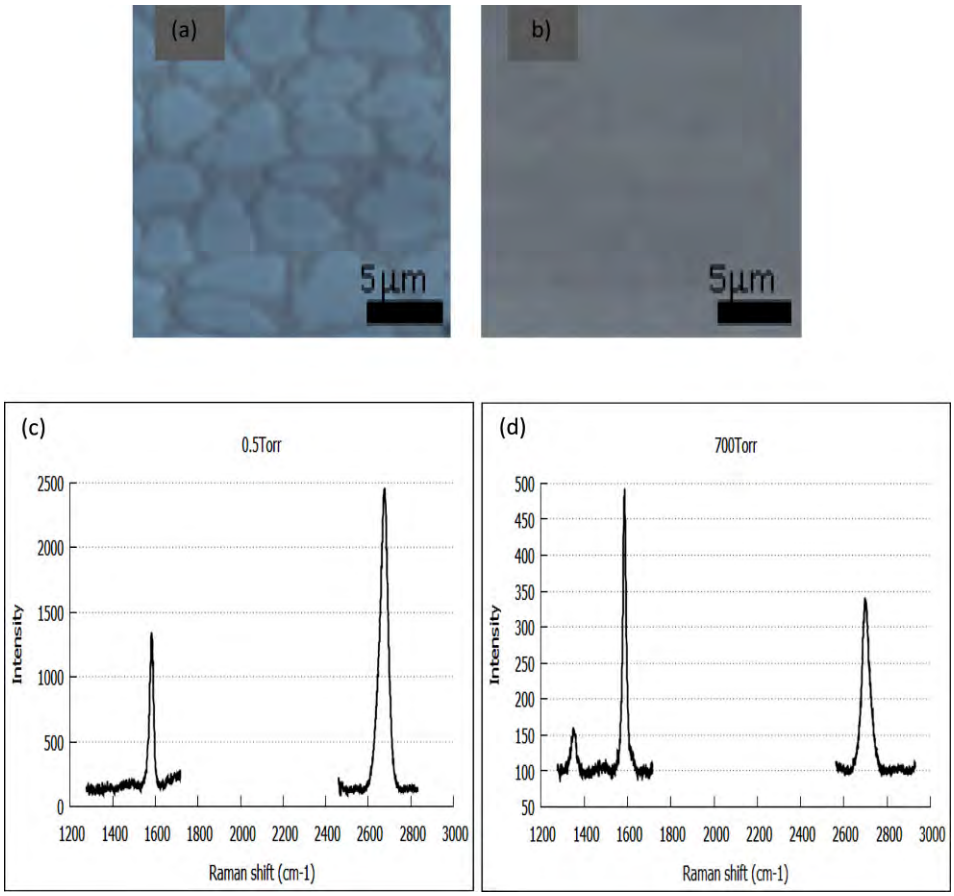

Fig. 1. Optical microscopy images of graphene synthesized under a) 0.5 Torr, b) 700 Torr. Raman spectra of graphene under c) 0.5 Torr, d) 700 Torr.

form and of micrometer size are present under 0.5 Torr, whereas the graphene layer is continuous under 700 Torr.

According to Raman analyses (Fig. 1c), under 0.5 Torr the intensity of the disorder-induced D peak ($\sim$1345 cm^{-1}) is very low, suggesting that graphene is highly crystalline.[12,14] The 2D ($\sim$2689 cm^{-1})/G ($\sim$1591 cm^{-1}) peaks ratio is close to 1.44, meaning that graphene is formed of one or two layers.[12,14] Under 700 Torr (Fig. 1d), graphene clearly presents more crystalline defects (I_D/I_G ratio equal to 0.14). Moreover, the I_{2D}/I_G ratio is lower, meaning that more graphene layers are present. Growth of multi-layers of graphene on Cu has frequently been observed under atmospheric pressure (AP)CVD conditions.[16,17] These results confirm that the self-limiting formation of graphene on Cu by CVD does not apply under all conditions.[15–19] Thus the total pressure, and more precisely the methane partial pressure, play a major role in the crystalline state, morphology, and thickness of graphene.

In order to analyze more precisely the influence of CH_4 partial pressure on the first steps of nucleation and growth of graphene, lower methane partial pressures (9, 19, and 38 mTorr) were studied under a total pressure of 0.5 Torr, by only varying the methane flow rate. Figure 2 shows a clear variation in the shape, size, and density of the graphene flakes. Indeed, a decrease in the carbon supply leads to a decrease of the nuclei density, as found by other authors.[20,21] Concomitantly, the average surface area of the nuclei increases, so the higher the graphene nucleation density, the smaller the graphene flakes. Our interpretation is that under high methane partial pressure, the amount of available reactive species leading to carbon adatoms is high enough to allow many nuclei to reach a thermodynamically stable size. Consequently, the nuclei density is high, but their size remains small since the carbon supply is limited. An increase in deposition time would lead to a continuous film of graphene on the copper surface, but this film would have many grain boundaries and thus poor physical properties.[22] For lower methane partial pressures, the amount of available carbon adatoms is smaller and fewer nuclei reach the stable size. The few stable nuclei collect more adatoms and become larger, probably because growth is more energetically favorable than nucleation.

Another interesting observation concerns the change in nuclei shape with the precursor partial pressure (Fig. 2). For 38 and 19 mTorr, a variety of shapes is observed, whereas under 9 mTorr, nuclei are multi-lobed with specific orientations. Several studies have obtained similar multi-lobed shapes for methane partial pressures close to or lower

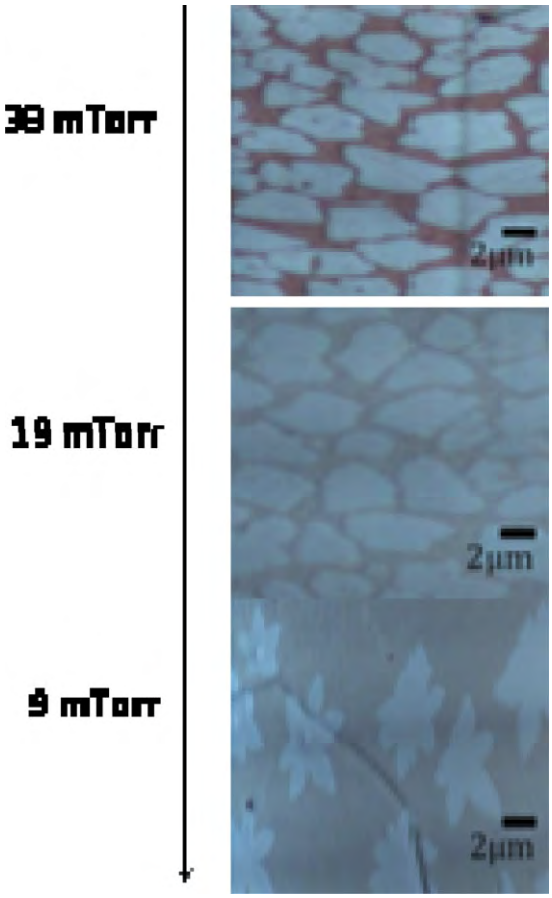

Fig. 2. Optical microscopy images of graphene synthesized under various methane partial pressures.

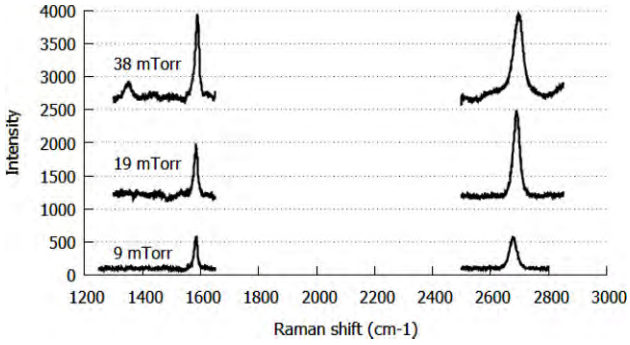

Fig. 3. Raman spectra of graphene synthesized under various methane partial pressures.

than ours.[19,22–25] For most of them, the multi-lobed nuclei are considered as a single nucleus. This variation in nuclei morphology could be the result of nuclei surface diffusion (Smoluchowski ripening process) thanks to weak carbon-copper bonds,[25] or of a competition between surface diffusion and preferential growth related to the lattice match between graphene and copper, as proposed by Wofford et al.[26] Other authors believe that the morphology of graphene nuclei can be tuned by varying the synthesis parameters, and is not influenced by the copper substrate.[19]

The Raman spectra presented in Figure 3 show an increase of graphene quality for lower precursor concentration, as deduced from the I_D/I_G ratios. The I_{2D}/I_G ratio indicates that 3–4 layers are obtained for the highest methane partial pressure, whereas only 1 or 2 layers are formed for the two other precursor concentrations. This is in agreement with the results of Luo et al.[27] Because of mass flow meter limitations, the methane partial pressures we used in these experiments were probably not low enough to allow the synthesis of strictly monolayer graphene flakes. Indeed, some authors succeeded in obtaining monolayer graphene flakes using methane concentrations of some ppm.[14,22]

During these experiments, thanks to the particular shape of the substrate holder (see Fig. 4a), a gradient in size, shape, and density of the nuclei was observed on the copper foil part located in the substrate holder slot, as presented in Figure 4b. The average density of nuclei is much lower and their average size is higher at the substrate bottom. When going to the top of the substrate, the nuclei become smaller and more numerous. On the part of the copper foil located outside the substrate holder slot, there is no more gradient in nuclei size and density.

To better understand this phenomenon, a grid of copper and another one of molybdenum were used to fully confine the copper substrate. Several runs were performed under 9 mTorr of methane using two Cu foils, one with confinement and the other one without grid. The results were similar with the Cu and the Mo grids, meaning that the effect of the grid was not catalytic. With enclosure, the graphene surface coverage of the Cu substrate is smaller and the nuclei are much more uniform in density and size over the entire substrate surface, as shown in Figures 5a and 5b. Moreover, the I_D/I_G ratios deduced from the Raman spectra given in Figure 5c are lower when a grid is used to enclose the copper foils, indicating a better graphene quality. The I_{2D}/I_G ratios are also higher with confinement (ratio equal to 2.5 with confinement and to 1.4 without), indicating a lower number of layers.

Comparable results were obtained by Li et al.[28] who used a copper foil enclosure as the substrate (i.e., they bent a 25 µm thick Cu foil and they crimped the three remaining sides) at 1035°C and under 50 mTorr of methane. Graphene grew on both sides of the substrate, but inside the enclosure, a much lower density of nuclei was obtained. Zhang et al.[19] developed a vapor-trapping method which consisted of installing a half inch quartz tube inside their two inch CVD reactor. A Cu substrate was then placed outside and inside the small quartz tube at 1000°C and under 15 mTorr of methane. Inside the small tube, mono- or bi-layer six-lobe graphene flowers of 100 µm size were formed whereas outside, graphene was continuous. In both studies, the variations in graphene characteristics were attributed to a much lower methane partial pressure inside the enclosure. In

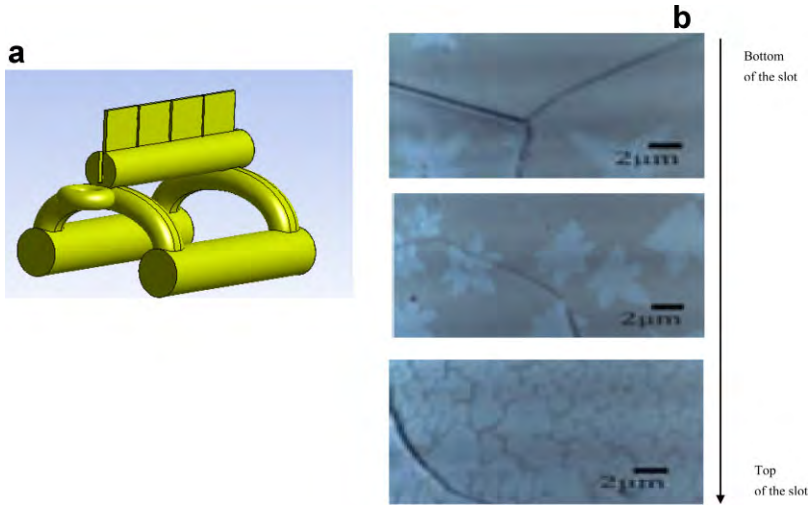

Fig. 4. a) Schematic representation of the substrate holder. b) Optical microscopy images of graphene flakes at various heights of the sample in the substrate holder slot under 9 mTorr of methane.

our study, this explanation is not valid since the substrate was not fully confined, considering that at 1000°C and under 0.5 Torr, gas diffusivities are high. We believe that the enclosure traps (i.e., makes disappear) a part of the reactive gaseous species involved in graphene formation, which could be formed either by methane pyrolysis or by catalytic phenomena related to the copper substrate. These gaseous species could be unsaturated molecules, as it will be detailed below.

The scanning electron microscopy (SEM) analyses made on samples synthesized with and without enclosure (Fig. 6), revealed another difference concerning the nuclei formation on both substrates. A dark circle is present in the middle of the nuclei on the encapsulated samples, whereas without confinement, the mono- or bi-layered nuclei are classically of uniform color on their entire surface. Raman analyses presented in Figure 7a were conducted at the center (called position 2 of Fig. 6b) and at the outer zone (position 1 of Fig. 6b) of a nucleus formed on an encapsulated sample. A much higher I_{2D}/I_G ratio was observed at position 1, indicating a lower number of layers and therefore the existence of multilayered nuclei. The crystalline quality is identical (low I_D/I_G ratios).

These results were confirmed by performing Raman mapping of the I_D/I_G and I_{2D}/I_G ratios on nuclei formed with and without enclosure, as detailed in the Supplementary Material. The uniformity of the I_D/I_G ratio clearly appears over the surface of the nuclei. Lower values are observed with enclosure. These mappings also confirm that, with enclosure, the nuclei have two distinct areas, a bi-layered one at the center of the nuclei and a monolayered one for the outer zone. Without enclosure, the nuclei are strictly bi-layered everywhere.

Similar results have already been obtained by Nie et al.[29] who pointed out that the underneath layer is the smallest one. For Vlassiouk et al.,[22] since these additional top layers appear in the middle of graphene nuclei, their formation likely occurs only at the beginning, when the amount of supplied active surface-bound carbon exceeds what can be consumed by the small perimeter of graphene nuclei. Upon reaching a large enough size, the amount of produced active carbon decreases due to a smaller area of open catalytic Cu, and it is mostly consumed by the first layer graphene which is the largest one. Indeed Kalbac et al.,[30] by using carbon isotopes, demonstrated that these multilayered nuclei are formed at an early stage. According to Han et al.[31] graphene bi-layered regions on copper can be attributed to the carbon segregation which occurs preferentially at defect sites upon cooling down. For Robertson and Warner,[32] graphene multi-layered flakes form at high levels of precursor supersaturation due to excess methane supply. For our experiments, our interpretation is that with and without enclosure, at the beginning of graphene formation since the catalytic Cu surface area is maximal, the carbon supply is certainly too high for the formation of only one graphene monolayer, as explained by Vlassiouk et al.[22] and Robertson and Warner.[32] Therefore, the nuclei present several layers. Without enclosure, even when the catalytic surface area decreases due to graphene formation, the amount of supplied carbon atoms is probably high enough to allow the growth of all the layers of the initial nuclei. Conversely with enclosure, a part of the active carbon atoms being consumed by the grid, their amount could not be sufficient to allow the growth of all the layers. Thus the enclosure allows the formation of better quality graphene with fewer layers because a part of the reactive gaseous species involved in graphene formation is consumed by the grid. This phenomenon is typical of CVD processes in which unsaturated species are involved, since they have a very high reactivity (sticking coefficient on solids equal to 1).[33] According to several studies,[18,22,25,34] unsaturated species are responsible for graphene formation. Vlassiouk et al.[22]

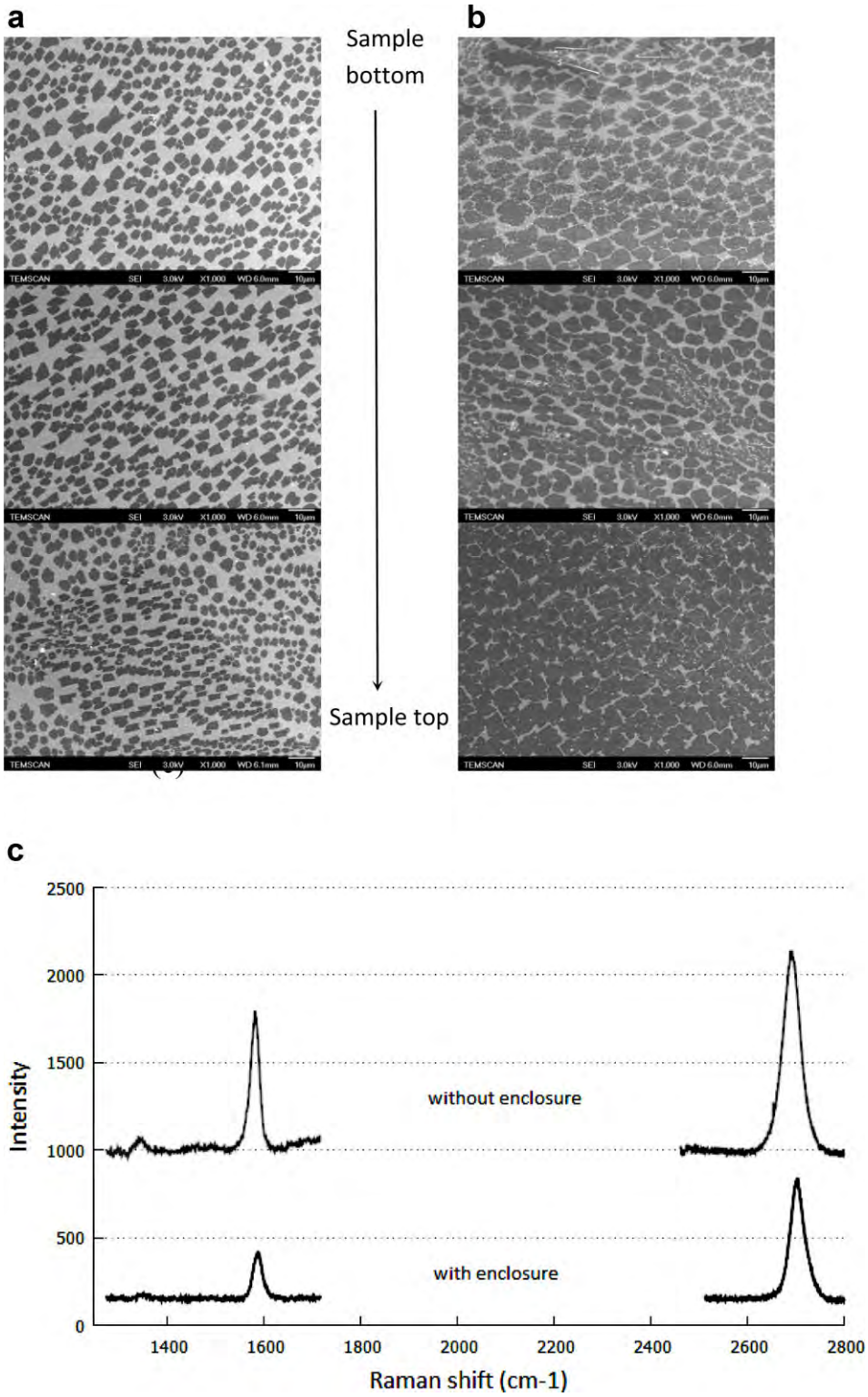

Fig. 5. Field emission gun (FEG) SEM views of nuclei evolution vs. the position on the sample a) with, and b) without enclosure. Raman spectra of graphene flakes obtained c) with and without enclosure.

proposed a mechanism assuming that the CH_3 methyl unsaturated species is the main molecule leading to graphene formation. The DFT calculations conducted by Li et al.[34] indicate that several unsaturated species, such as CH_3, C_2H_3, or C_2H_5 can be involved in graphene synthesis, depending on the position of the substrate in the reactor.

To get a better understanding of the unsaturated species potentially involved in graphene formation, the CVD

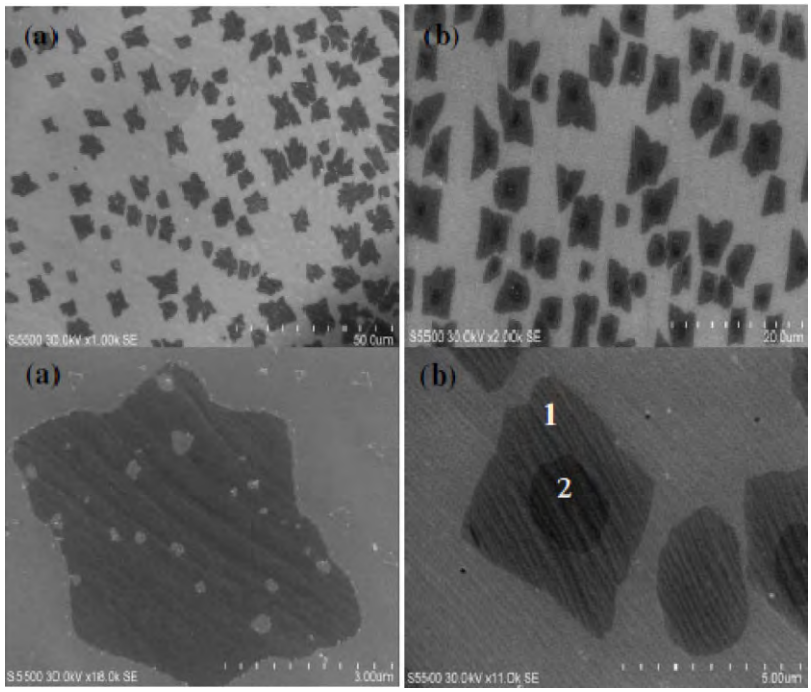

Fig. 6. FEG SEM views of graphene flakes obtained a) without, and b) with enclosure under 9 mTorr of methane.

reactor has been simulated using the commercial CFD software Fluent Ansys. The tubular reactor was assumed to be axisymmetric (the substrate holder and the copper foil were not considered). A specific function was used to implement the axial thermal profile obtained from experimental measurements along the reactor (the target temperature was obtained only after 37 cm from the reactor entrance and then on 42 cm along). Gases were considered as ideal. Steady state conditions were assumed. The aim was to analyze the gaseous species produced by methane pyrolysis during the CVD process, without considering any surface reaction or catalytic effect. The following chemical mechanism was implemented with the associated kinetic laws, taken from the very complete work of Holmen et al.[35]

$CH_4 \rightarrow CH_3 + H$	(R1)	$C_2H_2 + H \rightarrow C_2H + H_2$	(R11)
$CH_4 + H \rightarrow CH_3 + H_2$	(R2)	$C_2H_2 + CH_3 \rightarrow C_2H + CH_4$	(R12)
$CH_3 + CH_3 \rightarrow C_2H_6$	(R3)	$C_2H + H \rightarrow C_2H_2$	(R13)
$C_2H_6 + H \rightarrow C_2H_5 + H_2$	(R4)	$CH_3 + CH_3 \rightarrow C_2H_5 + H$	(R14)
$C_2H_6 + CH_3 \rightarrow C_2H_5 + CH_4$	(R5)	$C_2H_4 \rightarrow C_2H_3 + H$	(R15)
$C_2H_5 \rightarrow C_2H_4 + H$	(R6)	$C_2H_5 + C_2H_2 \rightarrow C_2H_6 + C_2H$	(R16)
$CH_3 + CH_3 \rightarrow C_2H_4 + H_2$	(R7)	$C_2H_5 + H \rightarrow C_2H_6$	(R17)
$C_2H_4 + CH_3 \rightarrow C_2H_3 + CH_4$	(R8)	$C_2H_4 \rightarrow C_2H_2 + H_2$	(R18)
$C_2H_4 + H \rightarrow C_2H_3 + H_2$	(R9)	$C_2H_3 + H \rightarrow C_2H_2 + H_2$	(R19)
$C_2H_3 \rightarrow C_2H_2 + H$	(R10)		

Nineteen chemical reactions and ten gaseous species are considered. Among the ten molecules, five species are unsaturated. The evolutions of the molar fractions of methane and of the unsaturated species along the reactor central axis are presented in Figure 8. The temperature of the isothermal zone was 1000°C, the flow rates were fixed at 8, 20, and 400 sccm for methane, hydrogen, and argon, respectively. Two total pressures, 0.5 and 700 Torr, were investigated.

First, the main result provided by this model is that, at 1000°C and for the two total pressures considered, CH_4 is decomposed in the gas phase to form saturated and unsaturated molecules, so even without a catalyst, unsaturated species are formed from methane pyrolysis, and could be involved in graphene formation. As a consequence, two types of unsaturated species could co-exist during graphene synthesis, the first one formed in the reactor volume as soon as the temperature of the gas is high enough to allow methane pyrolysis to occur, and the second one only formed at the vicinity of the copper surface, due to its catalytic activity. Thus, due to their very high reactivity, the first

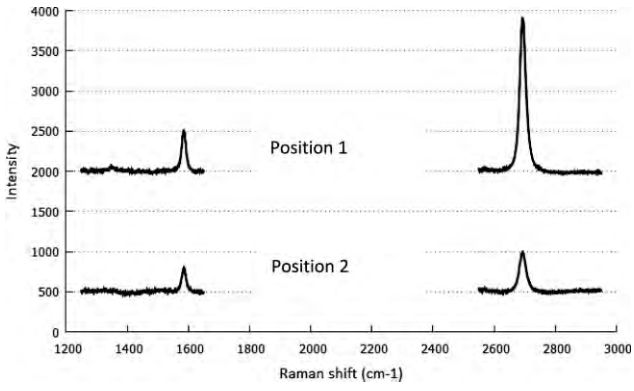

Fig. 7. Raman spectra at the center and at the outer zone of a graphene flake of an enclosed sample.

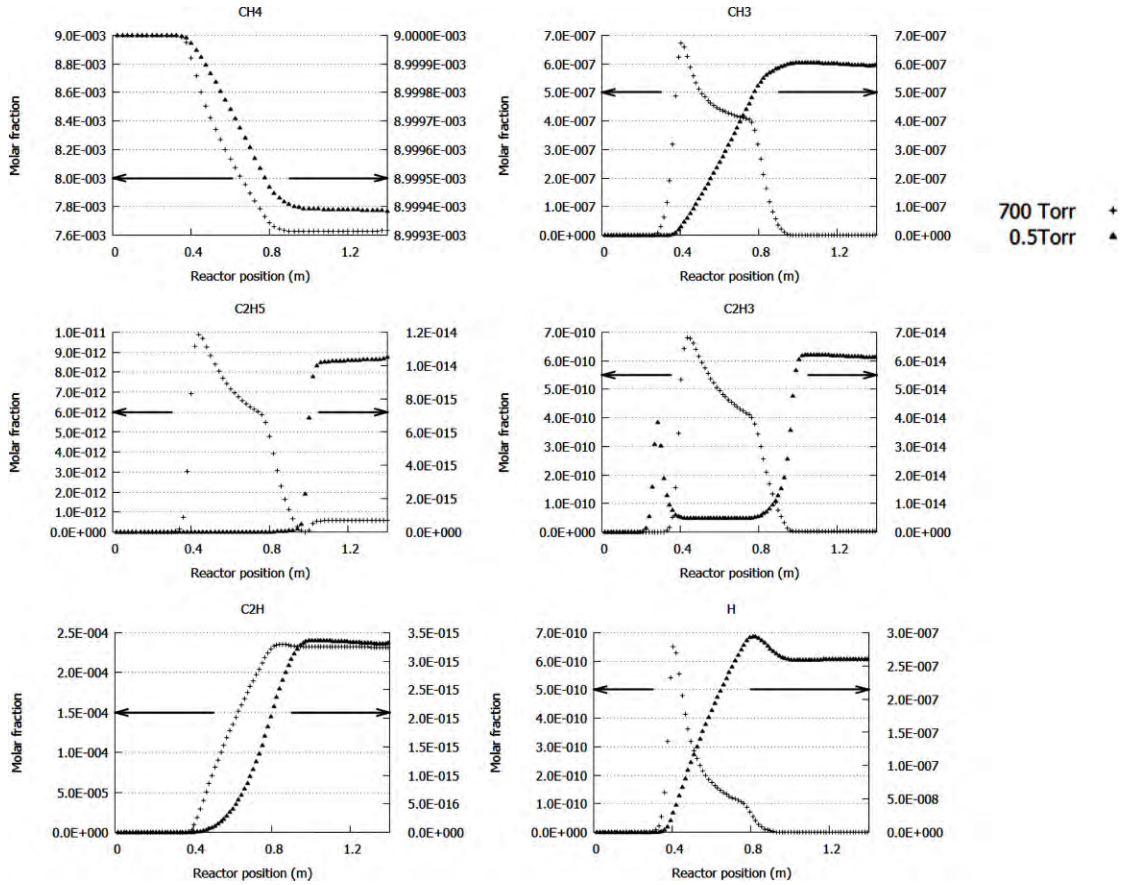

Fig. 8. Evolution of the molar fractions of methane and of the unsaturated species along the reactor axis under 0.5 and 700 Torr, calculated by the Fluent Ansys code.

type of unsaturated species (i.e., that produced by methane pyrolysis) could chemisorb onto the surface of either the substrate holder slot or of a cage, as previously discussed. This could reduce the amount of active carbon for graphene formation, leading to lower graphene surface coverage, fewer defects, and fewer layers.

If we compare the calculated results obtained under the two total pressures, an important difference regarding the methane conversion rate can be observed. Under low pressure, only 0.01% of methane is decomposed, whereas under 700 Torr, 15% of methane is converted. Under 0.5 Torr, only the two first chemical reactions are active (the concentration of the C_2 species is very low, and the corresponding reaction rates are close to zero), which explains that the molar fractions of CH_3 are strictly increasing along the reactor. In both conditions, the CH_3 methyl unsaturated species has molar fractions of a similar order of magnitude, but under 700 Torr, its partial pressure is 1,400 times higher. If we suppose that this molecule is the main precursor of graphene formation, as has already be mentioned in the literature,[18] this could explain that continuous multilayered graphene is much more easily formed under high methane pressure than under reduced pressure, where monolayered graphene flakes are often obtained.

It is worth noting that under 0.5 Torr, the H molar fraction is also strictly increasing along the reactor and the partial pressure ratio P_H/P_{CH3} is much higher than under 700 Torr, because reactions (R3) to (R19) are inactive under 0.5 Torr. The well-known etching role of H[22] could then be more pronounced under 0.5 Torr, explaining the higher crystallinity of graphene under low pressure.

Under 0.5 Torr, CH_3 is the most concentrated unsaturated species, whereas under 700 Torr, C_2H molar fractions are roughly 500 times higher than those of CH_3. If C_2H is active in graphene formation, it would lead to the simultaneous deposition of two carbon atoms. This could explain the differences observed in the number of graphene layers, and in the amount of defects under high and low methane partial pressures. This is also consistent with the results of Luo et al.[27] indicating that the main species involved in graphene formation can change depending on the precursor partial pressure.

3. Conclusions

The role of the gas phase in graphene formation by catalytic CVD from methane on copper foil was studied experimentally. A decrease of total pressure or of methane

partial pressure clearly permits a reduction in graphene nucleation on behalf of growth, and then the formation of larger graphene flakes with fewer layers and crystalline defects. The self-limiting formation of monolayered graphene on copper was not observed for the tested synthesis conditions. Gradients in size, density, and shape of graphene flakes were present in the part of the substrates located in the substrate holder slot, revealing a possible role of gaseous unsaturated species in graphene synthesis. This assumption was confirmed by additional experiments using copper substrates confined by a grid since, under these conditions, graphene is uniform on the whole substrate surface and presents a lower surface coverage and fewer defects.

To get a better understanding of the phenomena occurring in the gas phase, a chemical mechanism of methane pyrolysis was implemented in the CFD code Fluent to simulate the CVD reactor. The model shows that, at 1000°C, CH_4 is decomposed in the gas phase to form saturated and unsaturated species, meaning that two types of unsaturated species could co-exist during graphene synthesis, the first one produced in the reactor volume from methane pyrolysis, and the second one only formed at the vicinity of the copper surface, due to its catalytic activity. The existence of the first type of unsaturated species could explain the fact that graphene formation is not self-limiting under high methane partial pressure.

4. Experimental

The CVD reactor consists of a horizontal quartz tube of 1400 mm length and 50 mm inner diameter. A three zones furnace of 760 mm length surrounds the reactor. The 25 μm thick copper foils (99.999% Alfa Aesar, 1 cm × 2 cm) were placed in the central isothermal zone of the reactor, using a substrate holder which maintains them vertically during the process, as detailed below. They were heated to 1000°C in a 20 sccm H_2 and 400 sccm Ar flow and annealed for 20 min. Then 4 to 35 sccm of methane was introduced into the reactor over 5 to 10 min with the same Ar and H_2 flow rates. The samples were then cooled to room temperature with an average rate of 16°C min^{-1} under the same Ar/H_2 flow rates without methane. Raman spectroscopy (confocal Raman microscope Labram – Horiba Yvon Jobin with a laser excitation wavelength of 532 nm) and optical micrography were used to evaluate the thickness, crystalline quality, and uniformity of the graphene at room temperature. Each spectrum was obtained by five acquisitions of 30 s accumulation time. For each sample, at least nine Raman measurements were performed. Only the most representative Raman spectra are presented in the article. For most samples, coalescence of graphene flakes was not achieved, and Raman analyses were performed at the center of graphene flakes. For some samples, Raman mappings were performed. Spectra were collected every 0.8 μm in width and length. The autofocus was realized for every point to maximize the Raman response. Each spectrum was obtained by three acquisitions of 60 s accumulation time. All Raman analyses were conducted on graphene deposited on the copper foil, i.e., without transfer. The morphology of graphene films was analyzed using SEM (Jeol JSM 6700F and SEM Hitachi 5500).

[1] K. S. Novoselov, A. K. Geim, S. V. Morozov, D. Jiang, Y. Zhang, S. V. Dubonos, I. V. Grigorieva, A. A. Firsov, *Science* **2004**, *306*, 666.
[2] K. I. Bolotin, K. J. Sikes, J. Hone, H. L. Stormer, P. Kim, *Phys. Rev. Lett.* **2008**, *101*, 096802.
[3] C. Berger, Z. M. Song, T. B. Li, X. B. Li, A. Y. Ogbazghi, R. Feng, Z. T. Dai, A. N. Marchenkov, E. H. Conrad, P. N. First, W. A. de Heer, *J. Phys. Chem. B* **2004**, *108*, 19912.
[4] C. Berger, Z. M. Song, X. B. Li, X. S. Wu, N. Brown, C. Naud, D. Mayoun, T. B. Li, J. Hass, A. N. Marchenkov, E. H. Conrad, W. A. de Heer, *Science* **2006**, *312*, 1191.
[5] S. Park, R. S. Ruoff, *Nat. Nanotechnol.* **2009**, *4*, 217.
[6] A. Reina, X. Jia, J. Ho, D. Nezich, H. Son, V. Bulovic, M. S. Dresselhaus, J. Kong, *Nano Lett.* **2009**, *9*, 30.
[7] H. J. Park, J. Meyer, S. Roth, V. Skákalová, *Carbon* **2010**, *48*, 1088.
[8] V. V. Prakash, D. Santanu, L. Indranil, C. Wonbong, *Appl. Phys. Lett.* **2010**, *96*, 203108.
[9] W. Liu, H. Li, C. Xu, Y. Khatami, K. Banerjee, *Carbon* **2011**, *49*, 4122.
[10] Y. Lee, S. Bae, H. Jang, S. Jang, S. E. Zhu, S. H. Sim, Y. Song, B. H. Hong, J. H. Ahn, *Nano Lett.* **2010**, *10*, 490.
[11] S. Bae, H. Kim, Y. Lee, X. Xu, J. S. Park, Y. Zheng, J. Balakrishnan, T. Lei, H. R. Kim, Y. I. Song, Y. J. Kim, K. S. Kim, B. Ozyilmaz, J. H. Ahn, B. H. Hong, Z. Iijima, *Nat. Nanotechnol.* **2010**, *5*, 574.
[12] X. Li, W. Cai, J. An, S. Kim, J. Nah, D. Yang, R. Piner, A. Velamakanni, I. Jung, E. Tutuc, A. K. Banerjee, L. Colombo, R. S. Ruoff, *Science* **2009**, *324*, 1312.
[13] X. Li, W. Cai, L. Colombo, R. S. Ruoff, *Nano Lett.* **2009**, *9*, 4268.
[14] W. Wu, Q. Yu, P. Peng, Z. Liu, J. Bao, S. S. Pei, *Nanotechnology* **2012**, *23*, 035603.
[15] S. Lee, K. Lee, Z. Zhong, *Nano Lett.* **2010**, *10*, 4702.
[16] A. W. Robertson, J. H. Warner, *Nano Lett.* **2011**, *11*, 1182.
[17] Y. G. Yao, Z. Li, Z. Y. Lin, K. S. Moon, J. Agar, C. P. Wong, *J. Phys. Chem. C* **2011**, *115*, 5232.
[18] S. Bhaviripudi, X. Jia, M. S. Dresselhaus, J. Kong, *Nano Lett.* **2010**, *10*, 4128.
[19] Y. Zhang, L. Zang, P. Kim, M. Ge, Z. Li, C. Zhou, *Nano Lett.* **2012**, *12*, 2810.
[20] X. S. Li, C. W. Magnuson, A. Venugopal, J. An, J. W. Suk, B. Han, M. Borysiak, W. Cai, A. Velamakanni, Y. Zhu, L. Fu, E. M. Vogel, E. Voelkl, L. Colombo, R. S. Ruoff, *Nano Lett.* **2010**, *10*, 4328.
[21] H. Wang, G. Wang, P. Bao, S. Yang, W. Zhu, X. Xie, W. J. Zhang, *J. Am. Chem. Soc.* **2012**, *134*, 3627.
[22] I. Vlassiouk, M. Regmi, P. Fulvio, S. Dai, P. Datskos, G. Eres, S. Smirnov, *ACS Nano* **2011**, *5*, 6069.
[23] W. Wu, L. A. Jauregui, Z. Su, Z. Liu, J. Bao, Y. P. Chen, Q. Yu, *Adv. Mater.* **2011**, *23*, 4898.
[24] L. Liu, H. Zhou, R. Cheng, W. J. Yu, Y. Liu, Y. Chen, J. Shaw, J. X. Zhong, Y. Huang, X. Duan, *ACS Nano* **2012**, *6*, 8241.
[25] C. Hwang, K. Yoo, S. J. Kim, E. K. Seo, H. Yu, L. P. Biró, *J. Phys. Chem. C* **2011**, *115*, 22369.
[26] J. M. Wofford, S. Nie, K. F. McCarty, N. C. Bartelt, O. D. Dubon, *Nano Lett.* **2010**, *10*, 4890.
[27] Z. Luo, S. Kim, N. Kawamoto, A. M. Rappe, A. T. C. Johnson, *ACS Nano* **2011**, *5*, 9154.
[28] X. Li, C. W. Magnuson, A. Venugopal, R. M. Tromp, J. B. Hannon, E. M. Vogel, L. Colombo, R. S. Ruoff, *J. Am. Chem. Soc.* **2011**, *133*, 2816.
[29] S. Nie, W. Wei, S. Xing, Q. Yu, J. Bao, S. S. Pei, K. F. McCarty, *New J. Phys.* **2012**, *14*, 093028.
[30] M. Kalbac, O. Frank, L. Kavan, *Carbon* **2012**, *50*, 3682.
[31] Z. Han, A. Kimouche, A. Allain, H. Arjmandi-Tash, A. Reserbat-Plantey, S. Pairis, V. Reita, N. Bendiab, J. Coraux, V. Bouchiat, *Graphene* **2012**, arXiv :1205.1337.
[32] A. W. Robertson, J. H. Warner, *Nano Lett.* **2011**, *11*, 1182.
[33] I. Zahi, P. Mur, Ph. Blaise, A. Estève, M. Djafari Rouhani, H. Vergnes, B. Caussat, *Thin Solid Films* **2011**, *519*, 7650.
[34] Z. Li, W. Zhang, X. Fan, P. Wu, C. Zeng, Z. Li, X. Zhai, J. Yang, J. Hou, *J. Phys. Chem. C* **2012**, *116*, 10557.
[35] A. Holmen, O. Olsvik, O. A. Rokstad, *Fuel Process. Technol.* **1995**, *42*, 249.